

# Stereoselection at the Steady State. Group Selective Radical Cyclizations of Substrates Containing Two Radical Precursors and One Radical Acceptor

Dennis P. Curran,\* Chien-Hsing Lin, Nicholas DeMello, and Jörg Junggebauer

Contribution from the Department of Chemistry, University of Pittsburgh, Pittsburgh, Pennsylvania 15260

Received July 17, 1997

**Abstract:** The kinetic model for compound stereoselection presented in previous paper is verified experimentally by conducting a series of radical cyclizations of 1-(3-halo-2-(halomethyl)propyl)cycloalk-2-enecarboxylates with tributyltin hydride and measuring the ratios of products. Cyclization rate constants are abstracted from the data by an analysis that minimizes total error, and these rate constants compare favorably with rate constants that we measured directly on the corresponding monohalides. Transition state modeling was used to interpret the initial round of results and to design two new systems, one of which was predicted to cyclize with higher selectivity than the parent and the other of which was predicted to cyclize with reverse selectivity. These substrates bearing 4-*tert*-butyl groups were synthesized, and the experimental results verified the computational predictions.

## Introduction

The previous paper<sup>1</sup> outlined the conceptual basis for stereoselection at the steady state within the framework of group selective processes. At the steady state, the relative concentration of two stereomeric reactive intermediates remains constant. And if a concentration gradient between these two intermediates can be established, then they can be directed down different pathways that lead to the same product by choosing appropriate reaction conditions. The theory predicts, among other things, that by combining the natural convergent topography of a group selective process with the features of stereoselection at the steady state, it is possible to execute a net “group selective” transformation solely by using reaction topography. Two stereotopic reacting groups must be present in the precursor, but they need not react selectively to result in selective formation of a final product. This paper provides a series of experimental tests for the theory in the field of diastereotopic group selective radical cyclizations.

Radical cyclizations<sup>2</sup> were the first among several types of radical processes to receive attention from the standpoint of stereochemistry.<sup>3</sup> Most stereoselective radical cyclizations involve face selection; a radical folds into a suitable conformation to attack one face or the other of an alkene or related functional group. The Beckwith–Houk<sup>4,5</sup> model is a powerful tool to predict and rationalize the outcome of such cyclizations

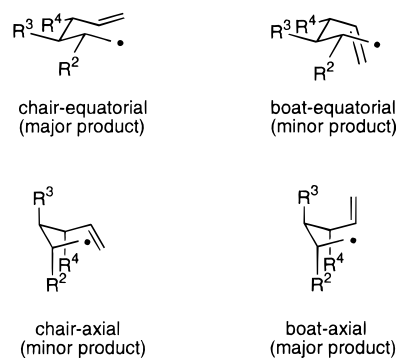


Figure 1. The Beckwith–Houk model.

that can be applied qualitatively or quantitatively.<sup>6</sup> In a qualitative approach, the major product of a 5-*exo* cyclization can often be predicted from the “chair-equatorial” model shown in Figure 1. Trends in stereoselection (including exceptions to the rule) can often be interpreted by comparing this chair with the alternative ring-flipped chair and boatlike models.

Group selective radical cyclizations are much less common than their face selective relatives.<sup>7</sup> Two general types of group selective radical cyclizations are possible: either there can be two radical acceptors and one radical precursor (class I) or there can be two radical precursors and one acceptor (class II). Interpretation of the results from class I (two acceptors) is generally straightforward. A key example that served as a design element in this work is shown in Figure 2.<sup>8</sup> Reductive

(1) Curran, D. P.; DeMello, N. *J. Am. Chem. Soc.* **1998**, *120*, 329.  
 (2) Review: Giese, B.; Kopping, B.; Gobel, T.; Dickhaut, J.; Thoma, G.; Kulicke, K. J.; Trach, F. In *Organic Reactions*; John Wiley & Sons Inc: New York, 1996; Vol. 48; p 301.  
 (3) (a) Curran, D. P.; Porter, N. A.; Giese, B. *Stereochemistry of Radical Reactions: Concepts, Guidelines, and Synthetic Applications*; VCH: Weinheim, 1996; p 283. (b) Chapter 2 of this book is a review of substrate controlled radical cyclizations.  
 (4) (a) Beckwith, A. L. J.; Easton, C. J.; Lawrence, T.; Serelis, A. K. *Aust. J. Chem.* **1983**, *36*, 545. (b) Beckwith, A. L. J.; Easton, C. J.; Serelis, A. K. *J. Chem. Soc., Chem. Commun.* **1980**, 482. (c) Beckwith, A. L. J.; Lawrence, T.; Serelis, A. K. *J. Chem. Soc., Chem. Commun.* **1980**, 484. (d) Beckwith, A. L. J.; Schiesser, C. H. *Tetrahedron Lett.* **1985**, *26*, 373.

(5) (a) Spellmeyer, D. C.; Houk, K. N. *J. Org. Chem.* **1987**, *52*, 959. (b) Broecker, J. L.; Houk, K. N. *J. Org. Chem.* **1991**, *56*, 3651.  
 (6) Examples: (a) Belvisi, L.; Gennari, C.; Poli, G.; Scolastico, C.; Salom, B. *Tetrahedron-Asymmetry* **1993**, *4*, 273. (b) Myers, A. G.; Condroski, K. R. *J. Am. Chem. Soc.* **1995**, *117*, 3057. (c) Takahashi, T.; Tomida, S.; Sakamoto, Y.; Yamada, H. *J. Org. Chem.* **1997**, *62*, 1912.  
 (7) (a) Curran, D. P.; Geib, S. J.; Lin, C. H. *Tetrahedron-Asymmetry* **1994**, *5*, 199. (b) Curran, D. P.; Shen, W.; Zhang, J. C.; Geib, S. J.; Lin, C. H. *Heterocycles* **1994**, *37*, 1773.

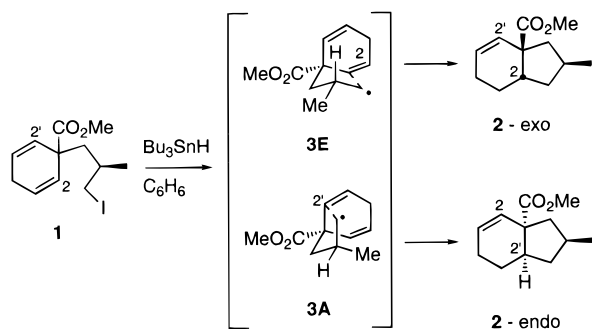


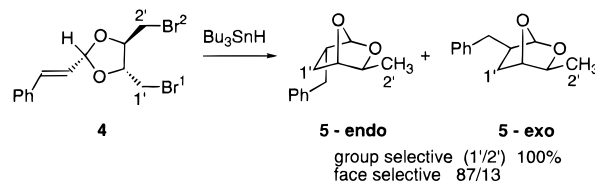
**Figure 2.** A class I group selective radical process: 2 acceptors and 1 precursor.

cyclization of **1** with tributyltin hydride provides **2-exo** and **2-endo** in temperature-dependent selectivities that range from 30/1 ( $-78\text{ }^{\circ}\text{C}$ ) to 15/1 ( $80\text{ }^{\circ}\text{C}$ ). The selectivity is established at the stage of the radical **3**, which chooses between a chairlike transition structure (**3E**) involving one olefin and an isomeric chairlike structure (**3A**) involving the other. It follows from a simple application of the Beckwith–Houk model that **3E** should be favored, and this prediction was borne out by the experimental results.<sup>8</sup>

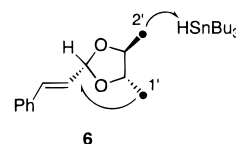
Although there are relatively few examples of this type of radical process,<sup>9</sup> it shows the usual features of other types of group selective reactions. Radical **3** makes a simple choice between one alkene and the other. Since both choices are intramolecular, the stereoselectivity of this process cannot be varied by changing the tin hydride concentration (although the ratio of directly reduced to cyclized products is of course affected by the tin hydride concentration). In this process, like most other group selective processes, there is no topological way to improve or erode the stereoselection; the only thing that counts is the relative energy of the competing transition states **3A** and **3E**.

More conceptually interesting is the class of reactions that has two radical precursors and one radical acceptor. According to the prior paper,<sup>1</sup> these reactions will exhibit a number of unusual features, including dependence of stereoisomer ratios on tin hydride concentration with the attendant ability to design reaction conditions that provide final product selectivities that exceed the level of selection in the group selective step.

There is at least one example of a group selective radical cyclization in class II that appeared prior to our work, and this is shown in Figure 3.<sup>10</sup> Reduction of dibromide **4** with tin hydride provides an 87/13 mixture of stereoisomers **5**. This process is completely group selective; the stereoisomer mixture results from the accompanying face selective process. The authors of this paper rationalized the result by positing the intermediacy of diradical **6**, which undergoes a group selective cyclization as shown. This would be a standard type of group selective process where two reactive entities directly compete for a single functional group; however, we are unaware of any group selective reactions of diradicals. In this mechanism, the problem is not with the postulate that the diradical **6** will undergo



Diradical rationale (untenable): both bromines are abstracted prior to cyclization



Topological rationale:  $\text{Br}^1$  and  $\text{Br}^2$  are abstracted non-selectively. The order of cyclization and reductive debromination is determined by which Br is abstracted.

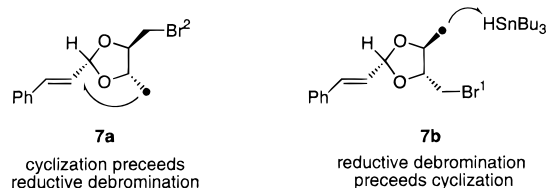


**Figure 3.** A class II group selective radical process: 2 precursors plus 1 acceptor.

stereoselective cyclization, it is with the postulate that diradical **6** will be generated in the first place. The reaction of a mono-radical with a second trialkyltin radical is a rare event because it is a radical–radical reaction, and when it does occur, it should provide the standard products of radical–radical reactions (coupling and disproportionation) rather than diradicals.

With 20/20 hindsight, we can now see that the reaction in Figure 3 is a superbly selective example of a class II group selective radical cyclization. If  $\text{Br}^1$  is abstracted (see **7a**), cyclization is possible because a normal “outside–outside” bicycle is formed. But if  $\text{Br}^2$  is abstracted (see **7b**), cyclization is impossible because an “inside–outside” fused dioxabicyclo-[2.2.1]heptane would result. The bromine abstraction surely occurs with little or no selection, but the reaction topography still dictates that the product is formed with complete group selection: if  $\text{Br}^1$  is abstracted first, then cyclization precedes reductive debromination, but if  $\text{Br}^2$  is abstracted first, then reductive debromination precedes cyclization. While ideal from a synthetic perspective, this process leaves something to be desired when viewed as a “proof” of our analysis of stereoselection at the steady state. The problem is that the disfavored cyclization is so slow that it could never occur under any conditions. So the proposed variation of stereoisomer ratios as a function of tin hydride concentration can never be tested. In other words, the slower of the two cyclizations is outside of the range when it can be affected by a third, independent process (tin hydride trapping).

To experimentally test the kinetic model for this type of topological group selective process requires the synthesis and study of a series of double radical precursors whose derived diastereomeric radicals cyclize over a range of different relative rates. Ideally, neither the faster nor the slower of the processes should be outside the range where it can be altered by changing the tin hydride concentration. We previously described a highly biased system with a  $k_f/k_s$  ratio of about 200, and showed that the experimental data fit the kinetic model.<sup>11</sup> Herein, we describe in detail a series of structurally related substrates that

(8) (a) Curran, D. P.; Qi, H. Y.; DeMello, N. C.; Lin, C.-H. *J. Am. Chem. Soc.* **1994**, *116*, 8430. (b) Qi, H. Ph.D. Thesis, University of Pittsburgh, 1995.

(9) Additional cyclization examples can be found in the following: (a) Reference 8b. (b) Lin, C.-H. Ph.D. Thesis, University of Pittsburgh, 1995. For group selective hydrogen transfer, see: (c) Sugimura, T.; Goto, S.; Koguro, K.; Futagawa, T.; Misaki, S.; Morimoto, Y.; Yasuoka, N.; Tai, A. *Tetrahedron Lett.* **1993**, *34*, 505. (d) Sugimura, T.; Koguro, K.; Tai, A. *Tetrahedron Lett.* **1993**, *34*, 509.

(10) Takano, S.; Ohashi, K.; Sugihara, T.; Ogasawara, K. *Chem. Lett.* **1991**, 203.

(11) Curran, D. P.; Qi, H. Y. *Helv. Chim. Acta* **1996**, *79*, 21.

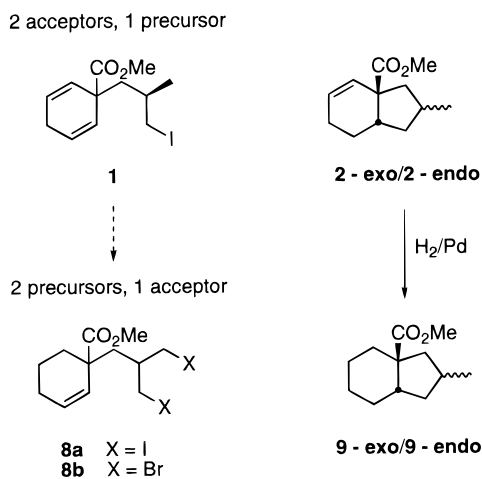


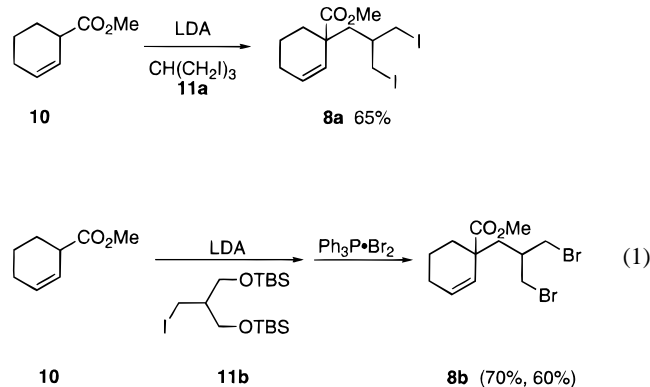
**Figure 4.** Designing a stereoconvergent group selective substrate.

provide  $k_f/k_s$  ratios ranging from just over 1 to about 10. A partial analysis of one of these substrates appeared in a preliminary communication.<sup>8a</sup> The ability of the kinetic model to fit the experimental data for a range of substrates with widely differing rates of cyclization and over widely different reaction conditions provides a strong validation of the kinetic model. In addition, our results provide new insight into the factors controlling stereoselection in radical cyclizations to cycloalkenes. Although these factors are presented in the context of group selection, they should be translated back to face selective processes that have similar features.

## Results and Discussion

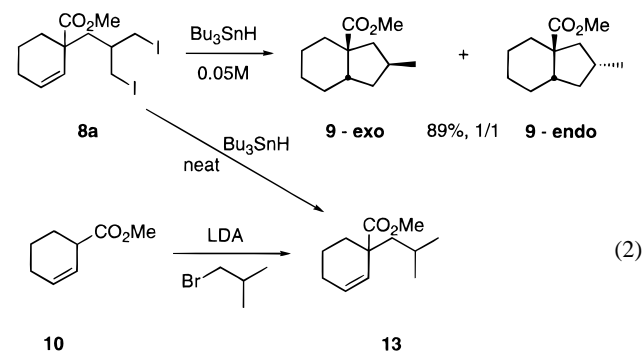
**Design and Study of a Stereoconvergent Group Selective Reaction.** The Class II substrates **8** were designed as shown in Figure 4 by the simple process of adding one radical precursor and deleting one radical acceptor from the class I substrate **1**. This approach has three attractive features: (1) the starting dihalides **8** should be readily available, (2) the configuration assignment of the products from its cyclization required only a simple one-step correlation to the products from **1**, and (3) the two diastereotopic radicals derived from **8** appeared to be so similar to the diastereomeric radical transition structures **3E** and **3A** derived from **1** (Figure 2) that we could readily predict that the rate constant ratio for the fast and slow cyclizations would be about 15. This prediction turned out to be wrong, but the substrate was nonetheless very informative.

To investigate the effect of different radical precursors and ring sizes, we prepared both dibromides **8b** and **14** and the diiodide **8a**. The diiodide was prepared directly in the remarkable alkylation shown in eq 1. Reaction of the enolate of **10**



with tris(iodomethyl)methane (**11a**) provided **8a** in 65% yield after flash chromatography. The reaction is remarkable because the triiodide **11a** appears to be ripe for a competing E<sub>2</sub> elimination process. The dibromides **8b** and **14** were prepared by alkylation of the enolate derived from **10** or **12** with the iodide **11b** followed by direct bromination of both (*tert*-butyldimethylsilyl) ethers.

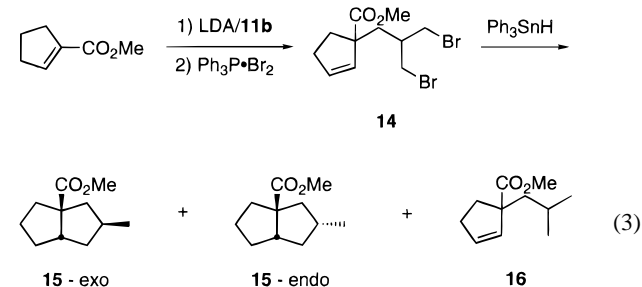
A preparative cyclization of the diiodide **8a** was first conducted with 2.5 equiv of tributyltin hydride (0.05 M). This provided an inseparable 1/1 mixture of **9-exo** and **9-endo** in high yield (eq 2). The structures were assigned by catalytic



hydrogenation of a 15/1 mixture of **2-exo** and **2-endo** to provide an authentic sample highly enriched in **9-exo** (Figure 4). The doubly reduced product **13** was available by reduction of **8a** with tin hydride at high concentration, but this product still contained **9-exo** and **9-endo**. More conveniently, alkylation of **10** with isobutyl bromide gave pure **13**.

With samples in hand and structures identified, cyclizations of the diastereotopic diiodide **8a** and dibromide **8b** were studied carefully. All the reactions were performed in benzene with *p*-dimethoxybenzene as an internal standard, a catalytic amount of AIBN, and an excess (10–15 equiv) of triphenyltin hydride in an oil bath at 75 °C. The <sup>1</sup>H NMR spectrum of the crude cyclized sample was obtained and it clearly showed three characteristic resonances: a doublet ( $\delta$  0.96) for the methyl group of the **9-exo**, a doublet ( $\delta$  1.01) for the methyl group of the **9-endo** product, and a “triplet” (actually two overlapping doublets centered at  $\delta$  0.84) for the methyl groups of the reduced product **13**. The yields of all the reactions were calibrated with the internal standard by <sup>1</sup>H NMR integration. In all cases, the total yields were 100 ± 5%, and for the purposes of comparison, the yields were calibrated to 100%.

Similar cyclizations of the cyclopentene dibromide **14** were conducted with triphenyltin hydride (see eq 3). In this case,



product ratios were more easily obtained from the GC chromatograms, but an NMR internal standard was still used in each case to ensure that the total yield of the three products was quantitative (100 ± 5%). Again, data are normalized to a total yield of 100%. Authentic samples of products were made by reactions similar to those in eq 2.

**Table 1.** Reduction of Diiodide **8a** with Ph<sub>3</sub>SnH

entry	Ph <sub>3</sub> SnH/ <b>8a</b>	[Ph <sub>3</sub> SnH]	9-exo	9-endo	13
1	2.6	0.02	53.0	47.0	
2	15.5	0.10	54.1	45.5	0.4
3	12.1	0.24	56.6	41.1	2.3
4	12.9	0.50	59.6	28.8	11.6
5	10.2	0.74	60.2	26.0	13.8
6	13.6	1.01	57.5	20.2	22.3
7	11.3	1.49	54.3	19.7	26.0
8	15.2	2.01	52.1	15.1	32.8

The data for reduction of **8a** are representative and are shown in Table 1. Tables 2 and 3 in the Supporting Information contain the data for **8b** and **14**. The data are plotted in Figure 6. These data show a number of unusual features for group selective processes. The ratio of exo to endo products at low tin hydride concentration is close to 50/50 in all three cases (entry 1, Table 1). This confirms that there is no selectivity in the abstraction of bromine or iodine by the tin radical, as expected. This also shows that there is no equilibration of radicals by bimolecular iodine transfer, a conclusion that can likewise be reached by comparing relative rates (radical cyclization is much faster than bimolecular iodine transfer).<sup>12</sup> As the tin hydride concentration increases, the yield of exo products begins to increase and the yield of endo products declines. Concomitantly, the doubly reduced products begin to grow in. After reaching a maximum in the vicinity of 60%, the yield of the exo product begins to decline, but the yield of the endo product declines more steeply, so the exo/endo ratio increases toward infinity as the combined yield goes to zero.

These data were analyzed within the mechanistic model shown in Figure 5 for the cyclohexane substrates. This is identical with the diastereoselective process presented in the preceding paper, so it is not discussed extensively. Briefly, at low tin hydride concentration, both the faster and the slower cyclizations of the two initially generated radicals **17x** and **17n** are faster than reduction by tin hydride. At this limit, the diastereoselectivity is controlled by the halogen abstraction step; since this is not selective, a 50/50 ratio of products forms. As the tin hydride concentration increases, both the faster **17x** and slower **17n** cyclizing radicals begin to be competitively trapped by tin hydride, opening new pathways that converge to the cyclized products or produce the doubly reduced product **13**. When the faster cyclizing radical **17x** happens to be reduced faster than cyclization, most of the resulting product **19** ultimately ends up at double reduction. But when the slower radical **17** is reduced, the resulting product **20** mostly follows the pathway to the major product **9-exo**. In this scheme, the yield of **9-exo** is then being both supplemented and eroded. But since the concentration of the slower cyclizing radical **17n** always exceeds that of the faster cyclizing radical, the yield of **9-exo** is supplemented faster than it is eroded.

We tried a number of approaches to extract rate constants from the data in these experiments. Newcomb's recommended rate constant for Ph<sub>3</sub>SnH was used for  $k_H$ .<sup>13</sup> Although some efforts were made to analyze all four rate constants ( $k_{f1}$ ,  $k_{f2}$ ,  $k_{s1}$ ,  $k_{s2}$ ) independently, this analysis is quite complicated, and it gave results that were intuitively unsatisfactory. The analysis

(12) Rate constants for iodine transfer between primary alkyl radicals are more than an order of magnitude lower than those from Ph<sub>3</sub>SnH, and Ph<sub>3</sub>SnH is also used in large excess. (a) Newcomb, M.; Sanchez, R. M.; Kaplan, J. *J. Am. Chem. Soc.* **1987**, *109*, 1195. (b) Newcomb, M.; Curran, D. P. *Acc. Chem. Res.* **1988**, *21*, 206. (c) Drury, R. F.; Kaplan, L. *J. Am. Chem. Soc.* **1972**, *94*, 3982.

(13) Newcomb, M. *Tetrahedron* **1993**, *49*, 1151.

is greatly simplified by making the assumption that the pairs of fast and slow rate constants are equal:  $k_{f1} = k_{f2} \neq k_{s1} = k_{s2}$ . This assumption seems intuitively reasonable. The only difference between the first and second cyclizations is that an iodomethyl (or bromomethyl) group is changed to a methyl group (compare **17x** to **21x** and **17n** to **21n**). It seems unlikely that this change will have a large effect on the rate constant. Furthermore, the satisfactory fitting of the data to the theoretical model (see below) provides additional support for this assumption.

After the two fast and slow rate constants are set as equal, the product functions in eqs 4–6 can then be used for the exo, endo, and reduced products, as derived in the prior paper.

$$[\text{exo}] = \frac{1}{2} \left\{ \frac{k_{\text{fast}}}{k_{\text{fast}} + k_{\text{H}}[\text{SnH}]} + \frac{k_{\text{fast}}}{k_{\text{fast}} + k_{\text{H}}[\text{SnH}]} \cdot \left( \frac{k_{\text{H}}[\text{SnH}]}{k_{\text{slow}} + k_{\text{H}}[\text{SnH}]} \right) \right\} \quad (4)$$

$$[\text{endo}] = \frac{1}{2} \left\{ \frac{k_{\text{slow}}}{k_{\text{slow}} + k_{\text{H}}[\text{SnH}]} + \frac{k_{\text{slow}}}{k_{\text{slow}} + k_{\text{H}}[\text{SnH}]} \cdot \left( \frac{k_{\text{H}}[\text{SnH}]}{k_{\text{fast}} + k_{\text{H}}[\text{SnH}]} \right) \right\} \quad (5)$$

$$[\text{reduced}] = \frac{1}{2} \left\{ \frac{k_{\text{H}}[\text{SnH}]}{k_{\text{slow}} + k_{\text{H}}[\text{SnH}]} \cdot \left( \frac{k_{\text{H}}[\text{SnH}]}{k_{\text{fast}} + k_{\text{H}}[\text{SnH}]} \right) + \frac{k_{\text{H}}[\text{SnH}]}{k_{\text{fast}} + k_{\text{H}}[\text{SnH}]} \cdot \left( \frac{k_{\text{H}}[\text{SnH}]}{k_{\text{slow}} + k_{\text{H}}[\text{SnH}]} \right) \right\} \quad (6)$$

A simple analysis of rate constant ratios with estimated values can now be made visually by using the functions derived in the prior paper as implemented by a program like MathCad. By “guessing” values of rate constant ratios (plotted against an arbitrary tin concentration), one finds (not shown) that the data nicely fit the predicted behavior for a  $k_f/k_s$  ratio in the range of 3–5. This is considerably lower than predicted in the “design” of the substrates outlined in the Introduction. Application of actual tin hydride concentrations to the plots then gives estimated rate constants. Although clearly supporting the analysis, this trial and error process is not satisfactory from the standpoint of accuracy and error estimation.

An independent computational approach was taken based on this trial and error approach. We first constructed an error function to calculate the agreement between the observed product ratios and the calculated product ratios for arbitrarily chosen values of  $k_f$  and  $k_s$  at a given tin hydride concentration. We then constructed a second function which summed the calculated error of all entries in Tables 1–3 for a given function and reported the total error. This “total error function” defines a surface whose range is all reasonable values of  $k_f$  and  $k_s$  and whose minimum indicates the most accurate choice of these values for the observed data. This type of fitting was computationally much more intensive and was accomplished on a UNIX cluster composed of four DEC system 5000's running a Mathematica 2.2 kernel under Ultrix 4.2A. Full details are provided in the Supporting Information along with a representative plot of this surface for the cyclization of **8a**.

The rate constants  $k_f$  and  $k_s$  derived from this analysis for all three substrates are shown in Figure 6. These calculated values can then be substituted into eqs 4–6 to generate theoretical lines

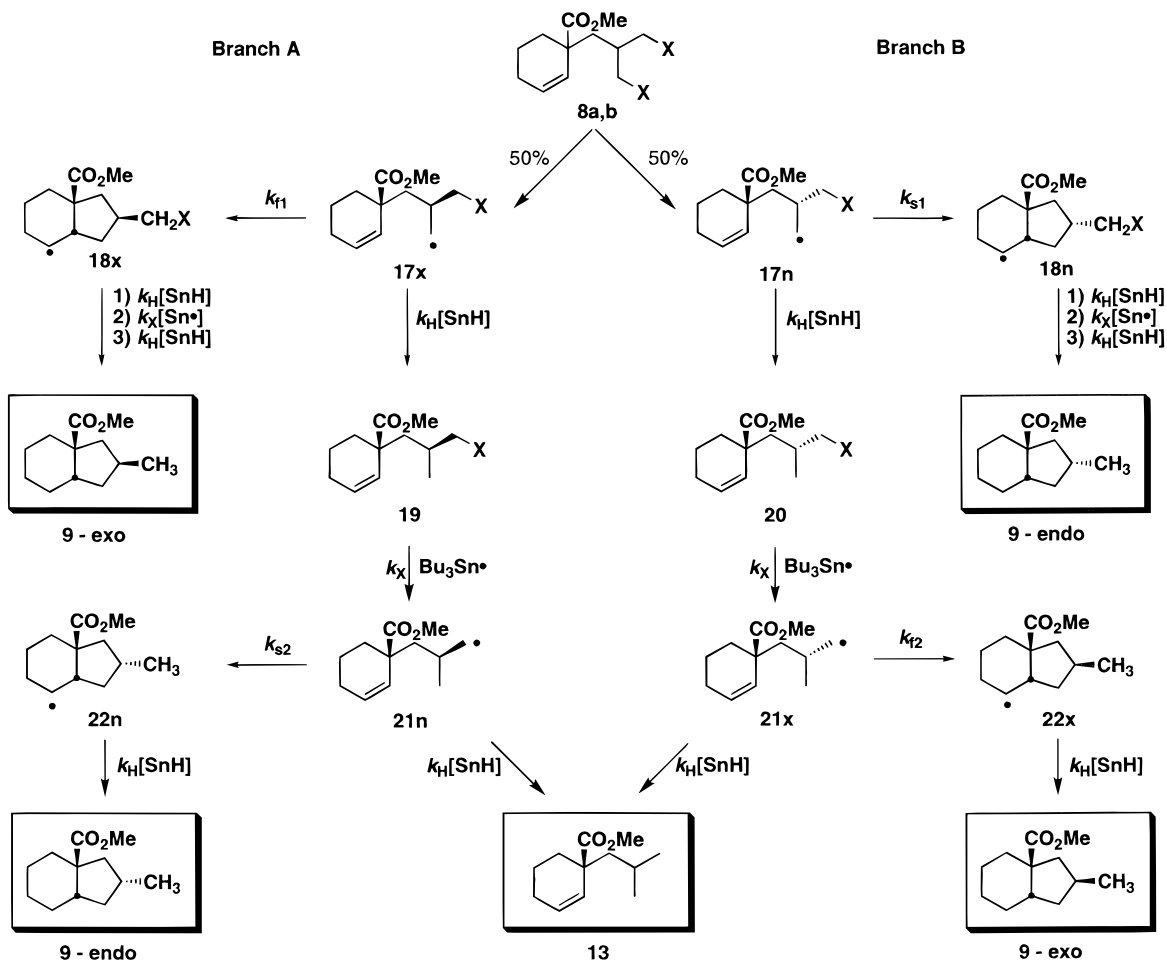


**Figure 5.** Mechanism of the topological group selective process.

for the yields of the corresponding products (exo, endo, reduced), and these lines are plotted against the actual data points in the graphs in Figure 6. It can be seen that the agreement between calculation (lines) and experiment (points) is excellent. The divergence of some points at very high tin hydride concentrations could be caused by a number of sources (for example, the pairs of rate constants may be similar, but not equal), but it may simply be an experimental problem; at these very high tin hydride concentrations (>50 vol % tin hydride), the concentration values are not very accurate. During the course of the research, this type of data analysis was actually conducted on incomplete data sets, and the predictions for missing values were confirmed by subsequent experiments.

There are several interesting features about the “best” rate constants (Figure 6) that emerge from the total error analysis. As deduced from the visual fitting, the ratios of rate constants are about 3–5; not 15 as predicted. Within the big picture of radical cyclizations, these rate constants are rather high. The parent hexenyl radical cyclizes with  $k_c = 10^6 \text{ s}^{-1}$  at  $80^\circ\text{C}$ . Even the slowest cyclizations in Figures 6 are more than 1 order of magnitude faster than this, no doubt due largely to the decreased rotational freedom of these radicals. Somewhat surprising is the observation that the cyclization to make the more strained bicyclooctane **15** (from **14**) is faster than the cyclizations to make the bicyclononanes **9** (from **8**). This trend is outside of experimental error, and can easily be seen by comparing actual data points. The last experimental point for the cyclization of **14** is virtually in neat tin hydride, and this is just barely past the concentration at which the maximum yield of **15-exo** is

observed. Even at this high concentration, the combined yield of cyclic products **15** is still 79%.

It is also interesting to compare the results of the dibromide **8b** and the diiodide **8a**. Within our analysis, these should provide identical rate constants even though the first pair of radicals (**17x,n**) is different ( $\text{X} = \text{Br}$  or  $\text{I}$ ). This is because the second pair of radicals (**21x,n**) is the same and because we assumed that the first and second pair had identical rate constants for cyclization. In our view, the differences between these pairs of numbers are too small to attribute an origin to the apparent error. The differences between these rate constants are not large based on standard indirect kinetic methods, and our analysis is even less direct than usual. While there could be small differences between the rate constant for cyclization of iodomethyl- and bromomethyl-substituted radicals **17x,n** ( $\text{X} = \text{Br}$  or  $\text{I}$ ), it is not safe to attribute the different rate constants obtained in **8a** and **8b** to this cause as opposed to any of a number of other experimental or analytical error factors.

To provide an independent confirmation of the rate constant analysis, we undertook the synthesis and kinetic analysis of the “half reaction” substrates shown in eq 7. These substrates are identical with those formed in the “second half” of the group selective reaction whenever the initial radical is reduced. If the first and second pair of cyclization rate constants are indeed identical, then the rate constants measured for these substrates should be identical with those in Figure 7. Ideally, the diastereomeric radical precursors **19** and **20** (or **23** and **24**) could be studied individually to provide unambiguous measurements of each of the slow and fast rate constants. In practice, it was

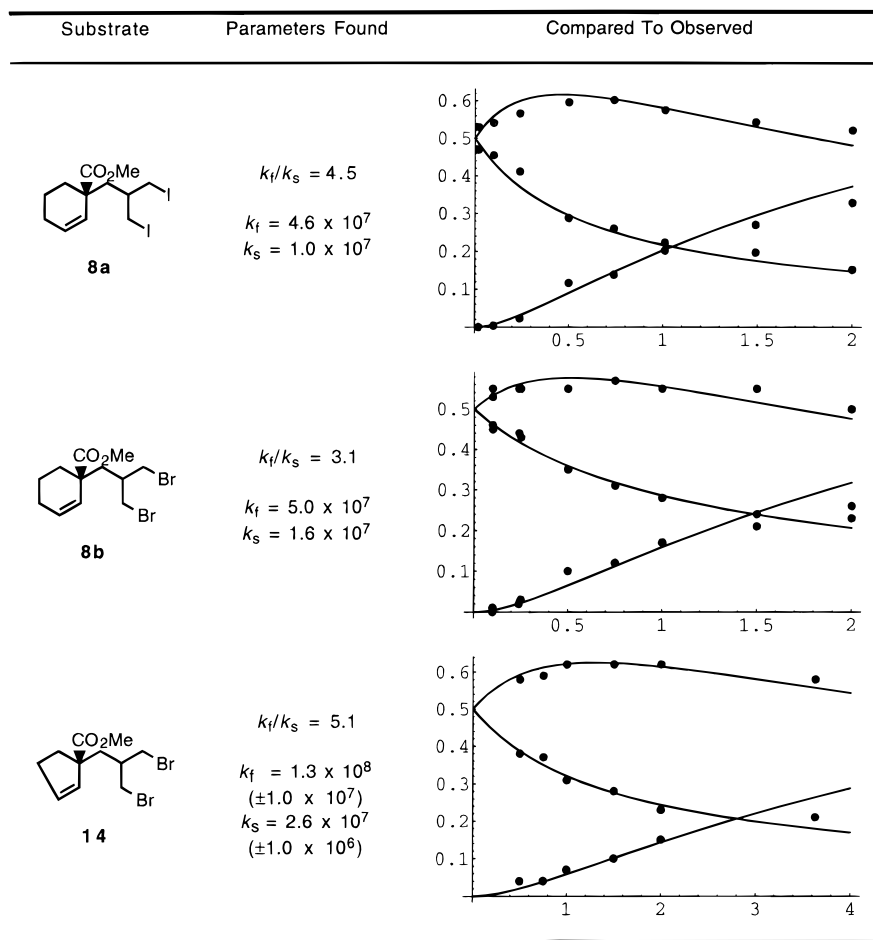
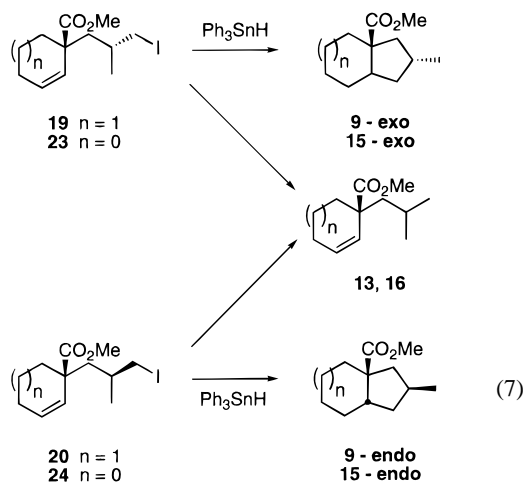
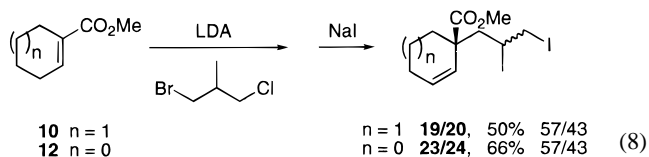


**Figure 6.** Fitting the data in Tables 1–3 with eqs 4–6. Data points were taken from Tables 1–3. Lines for exo, endo, and reduced products were calculated from eqs 4–6 with the indicated rate constants (in  $s^{-1}$ ). Product ratios are plotted against tin hydride concentration [M].

not possible to separate the diastereomers, so kinetic experiments had to be conducted on mixtures.

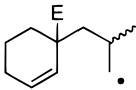
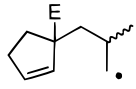


The substrates were prepared as shown in eq 8 as 57/43 diastereomeric mixtures. These results imply that there is a small kinetic resolution in the alkylation step. These mixtures were reduced in preparative experiments at low tin hydride concentrations to give 57/43 mixtures of exo/endo products. No doubly reduced products were formed. Kinetic experiments were conducted as described above, and the data for these experiments are shown in Tables 4 and 5 in the Supporting Information.



Knowing the ratio of the starting diastereomers (57/43), the rate constants for the fast and slow cyclizations in each mixture can then be extracted from the data by a relatively straightforward process that treats these as two independent reactions that give one product which is different (the cyclic product) and one product which is the same (eq 7). In this analysis, each individual data point provides a pair of rate constants that were then averaged over all the points to provide the “best estimate” rate constants shown in Figure 7. The agreement of these rate constants with those calculated in Figure 6 is only fair. In the case of the cyclohexene substrate, the calculated rate constants for the “half reaction” system are about 2–3 times lower than those from the full doubly convergent system, although the rate constant ratio of 4 is within the expected range. In the case of the cyclopentene system, there is good agreement with  $k_f$ , but  $k_s$  in the half reaction system is again low by about a factor of 2. Given the assumptions and the complexity of the systems involved, we feel that this level of agreement is reasonable.

**Computational Analysis of Transition States.** The studies with these substrates provided strong support for the model of group selection detailed in the preceding paper and in Figure 5 of this paper. But they also firmly showed that the actual level of selectivity in the group selective reactions of substrates **8**

	Ph <sub>3</sub> SnH	Bu <sub>3</sub> SnH	from dibromide <sup>a</sup> or diiodide <sup>a</sup>	Ph <sub>3</sub> SnH
	$k_f$ 1 X 10 <sup>7</sup>	2 X 10 <sup>7</sup>	5.0 X 10 <sup>7</sup>	4.6 X 10 <sup>7</sup>
	$k_s$ 3 X 10 <sup>6</sup>	4 X 10 <sup>6</sup>	1.0 X 10 <sup>7</sup>	1.6 X 10 <sup>7</sup>
	$k_f$ 7 X 10 <sup>7</sup>	1 X 10 <sup>8</sup>	1.3 X 10 <sup>8</sup>	
	$k_s$ 1 X 10 <sup>7</sup>	9.2 X 10 <sup>6</sup>	2.6 X 10 <sup>7</sup>	

<sup>a</sup> from Figure 7

**Figure 7.** Comparison of full-reaction with half-reaction rate constants (in s<sup>-1</sup>).

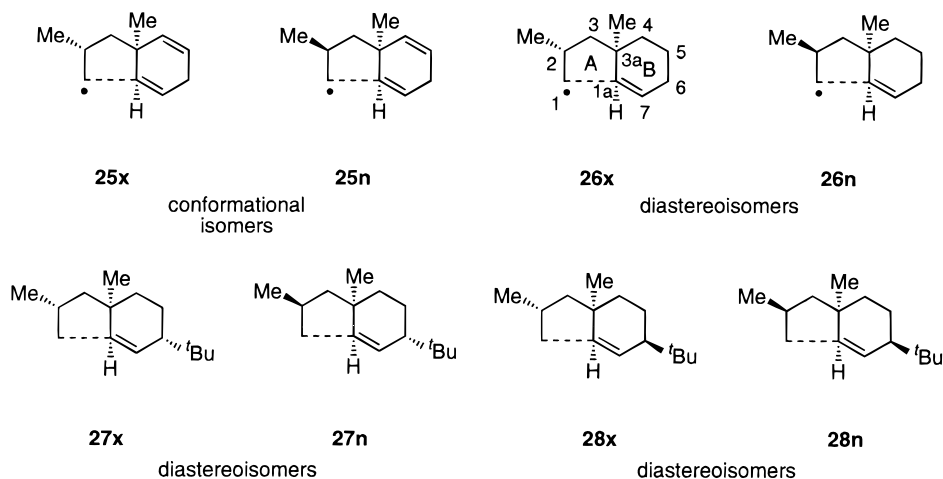


**Figure 8.** Models for transition state calculations.

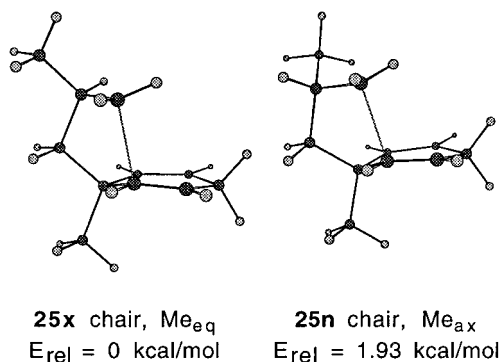
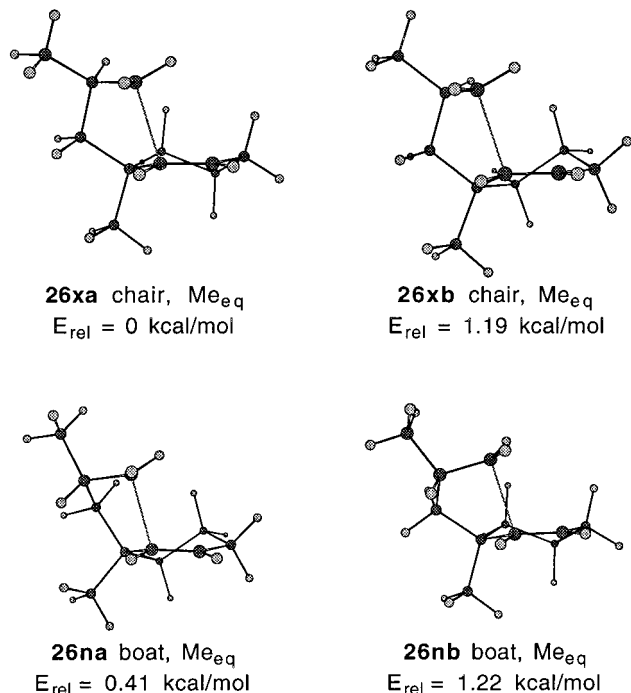
with two precursors and one acceptor was significantly lower ( $k_f/k_s = 4$ ) than that predicted by the model cyclization with two acceptors and one precursor ( $k_f/k_s = 15$ ). We undertook a series of calculations to gain insight into the reasons for the reduced selectivity and with the ultimate goal of designing a more selective substrate.

To decrease the number of possible transition states, we exchanged the ester group (which has several possible rotational isomers) for a methyl group (which has only one). This renders the results of the calculations more qualitative; however, the agreement of theory and calculation turned out to be remarkably good. The substrates studied are shown in Figure 8. Dienes **25x** and **25n** are conformational isomers and are direct models of **1** (Figure 4); however, they are drawn throughout the analysis as enantiomers to facilitate a constant view of the cyclohexadiene ring. Radicals **26x** and **26n** model the cyclizations in the group selective process. Therefore, these radicals are not conformational isomers but diastereoisomers. The direct comparison of the transition state energies of diastereomers is usually not especially meaningful because the transition states are not in competition with each other. However, the presence of tin hydride places these two transition states in competition in the process in Figure 5, so we simply compare the calculated diastereomeric transition state energies directly as if they were conformational isomers. These calculations do not provide direct isomer ratios, but they do provide rate ratios that can be compared to the experimentally measured rate constants. Inherent in this comparison is the assumption that the ground states of the two diastereomers **26x** and **26n** are equal in energy. This

is not generally a good assumption, but in this specific case it should be reasonable since the ground states only differ by the interchange of a “CH<sub>3</sub>” and a “CH<sub>2</sub>” group substituted on a common stereogenic carbon atom.

The calculations are described in detail and analyzed more fully in the Supporting Information. Here we present only the salient features for analysis of the group selection process along with the predictions and conclusions that emerge. Briefly, random geometries of the transition states were generated with Monte Carlo simulation and optimized by using the Houk–Spellmeyer molecular mechanics parameters for radical cyclization. Molecular orbital descriptions were created from the resulting geometries by ab initio techniques, and the transition state nature of the geometries was confirmed by quantum mechanics frequency calculations of the molecular orbital descriptions. Predicted isomer ratios were then generated by applying Boltzmann distribution functions to all transition state structures within 5 kcal/mol of the lowest energy one.

The two lowest energy transition states for **25** are shown in Figure 9. The lowest energy transition structure leads to the *exo* product, as expected from the results in Figure 2: the forming cyclopentane ring is “chairlike” with an equatorial methyl group (hereafter called “chair-Me<sub>eq</sub>”). Correspondingly, the higher transition structure (TS) leads to the *endo* product and is of the chair-Me<sub>ax</sub> type. A corresponding “boat-Me<sub>eq</sub>” TS leading to the *endo* product along with two other similar transition states leading to the *endo* product were also located (not shown). No other TSs leading to the *exo* product were

Figure 9. Low energy transition structures of **25**.Figure 10. Low energy transition structures of **26**.

located. The predicted Boltzmann distribution of exo/endo products is 14/1, which is remarkably close (perhaps fortuitously close, considering the structure change) to the observed ratio with **1**.

In contrast, analysis of the group selective system **26** provided seven transition structures. Of these, the two (of three) lowest energy structures of **26x** are shown in Figure 11 along with the two (of four) lowest energy structures from **26n**. Working with only these four structures (inclusion of the three higher energy TSs has little effect), the predicted ratio of exo to endo products is 1.6/1. The calculations clearly reflect the decreased selectivity in moving from **25** to **26**, although now the calculated level of selectivity is lower than that observed (about 4/1).

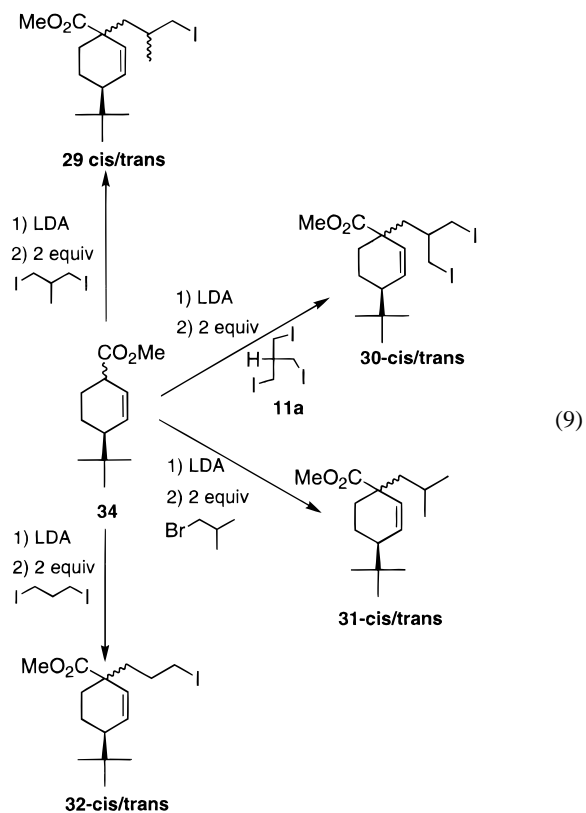
Both TSs leading to the exo product are of the “chair-Me<sub>eq</sub>” type; they differ in the direction of twist of the cyclohexene ring. In the lower energy transition state **26xa**, the side chain bearing the radical is pseudoequatorial while the higher energy TS **26xb** has this group pseudoaxial. The TSs leading to the endo product are both “boat-Me<sub>eq</sub>” with different half chair conformations of the cyclohexene: **26na** has a pseudoequatorial side chain while **26nb** is pseudoaxial. The radical transition states with the “chair-Me<sub>ax</sub>” geometry are prohibitively high in energy because they place the *endo*-Me group directly over the cyclohexene.

A straightforward prediction arises from these calculations: destabilizing TS structure **26na** should increase the stereoselectivity. This was done first in computations and then in experiments by placing a *tert*-butyl group in the 4-position *trans* to the side chain bearing the radical. This will destabilize the lower energy endo TS (**26na**) and the higher energy exo TS (**26xb**), which would now require axial *tert*-butyl groups.

This simple analysis was reflected in the calculations of **27x** and **27n**. Although eight different transitions were located (four for **27x** and four for **27n**), only two of these were close enough in energy to contribute significantly to the product distribution. These are shown in Figure 11. As anticipated from the analysis, the calculated ratio of rates has now increased to 8/1.

It was of special interest to calculate the results of the *cis* stereoisomer **28**, and these results are summarized in Figure 12. In the simple analysis, the favored transition states become **28xb** and **28na**, and this predicts that the selectivity in the cyclization should be reversed. Although this may seem surprising, it is actually expected. Analogy has been drawn between related bicyclic transition states and *cis*-decalins.<sup>14</sup> The flipping of the six-membered ring (induced by the *tert*-butyl group) also flips the forming five-membered ring and reverses the product configuration. The calculations with **28** provided four exo TSs and two endo TSs, but the lowest one of each taken together (see Figure 12) accounted for more than 94% of the products. The calculated product ratio is 5/1 and the endo isomer is indeed predicted to be favored.

**Experimental Testing of Computational Predictions.** The requisite samples to test the computational predictions were prepared as shown in eq 9. Alkylation of the enolate derived



from **34** with the various alkylating agents gave mixtures of *cis* and *trans* isomers of the corresponding products **29–32**. In



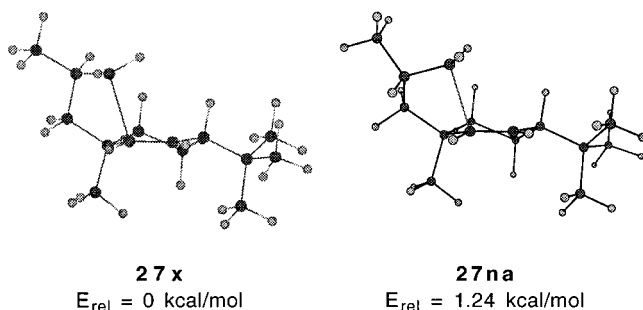


**Figure 11.** Low energy transition structures of **27**.

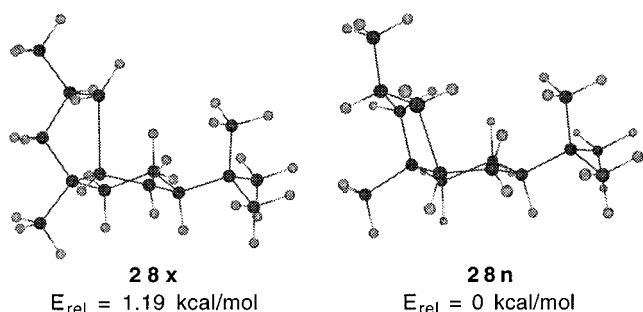
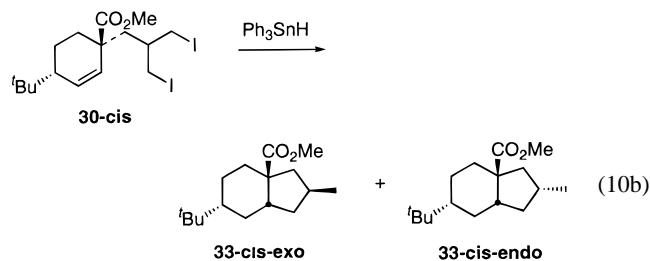
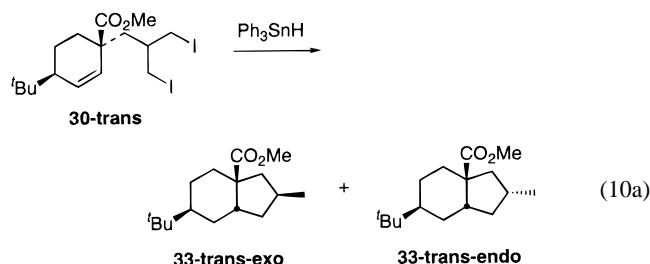


**Figure 12.** Low energy transition structures of **28**.

all cases, these isomers were separable by chromatography. Details of the synthesis, separation, and characterization of all these products are contained in the Supporting Information.

Isomers **30-trans** and **30-cis** were first cyclized in preparative experiments at low tin hydride concentrations to provide authentic samples of the respective exo and endo products (eq 10). Both reactions provided 50/50 mixtures of diastere-



omeric cyclic products **33** in excellent purified yields and free from the doubly reduced product **31**. The exo/endo configuration of the cis isomers was determined by hydrolysis of these compounds to the corresponding crystalline acids **37**, whose structures were solved by X-ray crystallography (see Supporting Information). These crystal structures also proved that the configuration in the alkylation was assigned correctly. The exo/endo configuration of the trans isomer of **33** was assigned by a series of qualitative spectroscopic correlations between the known compounds (**9-exo** and **9-endo**) and the corresponding isomers of **33-cis**.

Kinetic experiments with both **30-trans** and **30-cis** were conducted as before, and the data for these experiments are shown in Tables 6 and 7 in the Supporting Information and plotted with the usual analysis in Figure 13. The data in Figure 13 clearly show that the predictions of the calculations have been borne out in experiment. The plot of the **30-trans** shows increased selectivity compared to the parent **8**. For example, at 0.46 M concentration of tin hydride, the yield of **33-trans-exo** has increased from 50% to its maximum of 74% while the yield of **33-trans-endo** has declined from 50% to 19%; the remaining 7% is the double reduction product **31**. The rate constant  $k_f$  leading to the exo product is almost the same as that in the parent, while the rate constant  $k_s$  is lower than that in the parent. The experimental ratio  $k_f/k_s$  of 11 is higher than the parent and is close to the ratio of 8 predicted by the calculations.

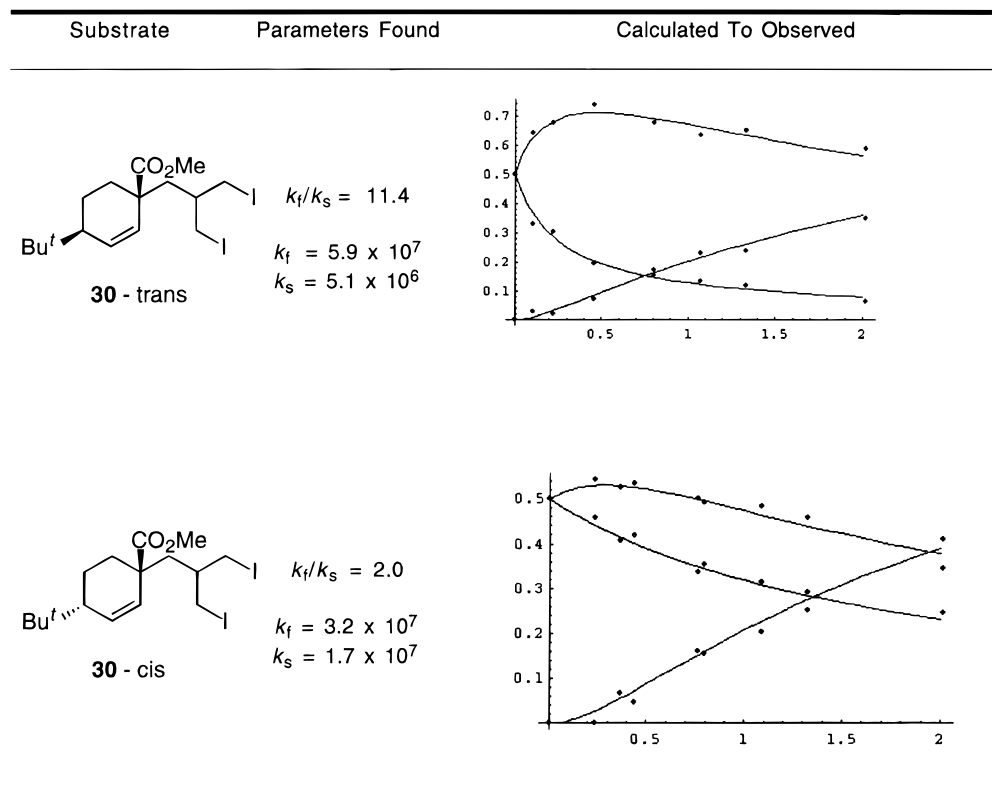
Perhaps even more impressive are the results with **30-cis**. As predicted by the calculations, the endo isomer is indeed the favored product; however, the predicted selectivity of 5 is not borne out by experiment. The ratio of the two rate constants is only about 2, and this is reflected in the gentle curvature of the lines in Figure 13.

The rate constants of the corresponding half-reaction models were again measured on mixtures of isomeric precursors **29-cis** and **29-trans**. The process was similar to that described above and the full details are provided in the Supporting Information. Figure 14 shows the “best” rate constants that emerge from this analysis. In the case of the **29-trans** isomer, the half-reaction rate constants agree reasonably well with the rate constants in Figure 13. In the case of **29-cis**, however, the two rate constants are calculated to be about equal. We feel that this is unlikely to be true and it is probably an error caused by the fact that the two rate constants in the mixture being measured are too close to resolve. Ideally, it would be better to separate the two diastereomers of **29-cis** and **29-trans** and measure the half reaction rate constants separately; however, in no case was separation evident during analytical or preparative chromatography of the precursors.

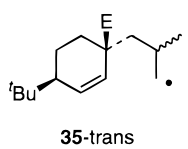
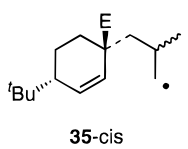
Last, the two model substrates **32-cis** were prepared to study the effect of the methyl group on the rate constant for cyclization. There is no issue of stereoselection in these molecules (aside from the formation of a cis/trans ring fusion); the analysis is made by comparing absolute rate constants. The absolute rate constants are easily measured by standard competition kinetics against tin hydride (data in Supporting Information) and are shown in Figure 15. Interestingly, both model compounds cyclize significantly more slowly than the slower of the two methyl-bearing diastereomers. Thus, in a formal sense, the replacement of either hydrogen at C2 of the propyl chain of **29** accelerates the radical cyclization; selectivity arises because one cyclization is accelerated more than the other. This trend presumably has its origins in the “Thorpe–Ingold” effect. In addition, we learn from these models that there is a very slight preference for cyclization of an equatorially oriented side chain over an axially oriented one. It is this low preference that is responsible for the relatively low selectivities obtained with substrates **8**.

## Conclusions

The experimental results described in this paper strongly support the model for compound stereoselection at the steady state that was put forth in the preceding paper.<sup>1</sup> The model has been used both qualitatively to interpret the stereoselection



**Figure 13.** Fitting the data in Tables 6 and 7 with eqs 4–6. Data points were taken from Tables 6 and 7. Lines for exo, endo, and reduced products were calculated from eqs 4–6 with the indicated rate constants (in  $s^{-1}$ ).

 <b>35-trans</b>	from "half-reaction"	from "full-reaction" <sup>a</sup>
	$k_f$ $3.4 \times 10^7$ $k_s$ $4.2 \times 10^6$	$5.9 \times 10^7$ $5.1 \times 10^6$
 <b>35-cis</b>	from "half-reaction"	from "full reaction"
	$k_f$ $1.7 \times 10^7$ $k_s$ $1.6 \times 10^7$	$3.2 \times 10^7$ $1.7 \times 10^7$

a. From Figure 14

**Figure 14.** Comparison of full-reaction rate constants with half-reaction rate constants (in  $s^{-1}$ ).

as a function of tin hydride concentration and quantitatively to extract relevant rate constants. The measured rate constants provide insights into the factors that control both rate and stereoselectivity in radical cyclizations to cycloalkenes. More importantly, the success of the kinetic model in interpreting the results leads us to conclude that stereoselection at the steady state is a general process, and that the concepts and kinetic equations outlined in part 1 can now be used to design substrates and interpret results for other kinds of complex steady state processes. The type of process outlined in this paper is by far the simplest, and other processes involving only bimolecular

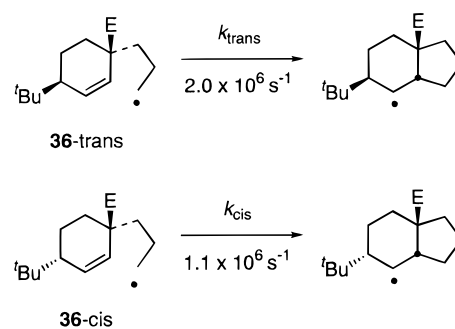


**Figure 15.** Model cyclizations lacking the methyl group.

reactions and/or catalytic reagents present significant challenges to experimental radical chemistry and other fields.

**Acknowledgment.** We thank the National Science Foundation for funding this work. Dr. Jörg Jungbauer thanks the Deutsche Forschungsgemeinschaft for a postdoctoral fellowship. We thank Dr. Marcelo Preite for help in preparing the manuscript.

**Supporting Information Available:** Full experimental and characterization data for all compounds, details of the error analysis and calculations, and details of the two crystal structures (55 pages). See any current masthead page for ordering and Internet access instructions.

JA9724102